A comparative investigation of Lu_2SiO_5:Ce and Gd_2O_2S:Eu powder scintillators for use in x-ray mammography detectors

2009 Meas. Sci. Technol. 20 104008

(http://iopscience.iop.org/0957-0233/20/10/104008)

Meas. Sci. Technol. **20** (2009) 104008 (9pp) doi:10.1088/0957-0233/20/10/104008

A comparative investigation of Lu_2SiO_5:Ce and Gd_2O_2S:Eu powder scintillators for use in x-ray mammography detectors

C M Michail[1], G P Fountos[2], S L David[1], I G Valais[2], A E Toutountzis[1], N E Kalyvas[2], I S Kandarakis[2] and G S Panayiotakis[1]

[1] Department of Medical Physics, Medical School, University of Patras, 265 00 Patras, Greece
[2] Department of Medical Instruments Technology, Technological Educational Institution of Athens, Egaleo, 122 10 Athens, Greece

E-mail: panayiot@upatras.gr

Received 15 December 2008, in final form 9 June 2009
Published 4 September 2009
Online at stacks.iop.org/MST/20/104008

Abstract
The dominant powder scintillator in most medical imaging modalities for decades has been Gd_2O_2S:Tb due to the very good intrinsic properties and overall efficiency. Apart from Gd_2O_2S:Tb, there are alternative powder phosphor scintillators such as Lu_2SiO_5:Ce and Gd_2O_2S:Eu that have been suggested for use in various medical imaging modalities. Gd_2O_2S:Eu emits red light and can be combined mainly with digital mammography detectors such as CCDs. Lu_2SiO_5:Ce emits blue light and can be combined with blue sensitivity films, photocathodes and some photodiodes. For the purposes of the present study, two scintillating screens, one from Lu_2SiO_5:Ce and the other from Gd_2O_2S:Eu powders, were prepared using the method of sedimentation. The screen coating thicknesses were 25.0 and 33.1 mg cm^{-2} respectively. The screens were investigated by evaluating the following parameters: the output signal, the modulation transfer function, the noise equivalent passband, the informational efficiency, the quantum detection efficiency and the zero-frequency detective quantum efficiency. Furthermore, the spectral compatibility of those materials with various optical detectors was determined. Results were compared to published data for the commercially employed 'Kodak Min-R film-screen system', based on a 31.7 mg cm^{-2} thick Gd_2O_2S:Tb phosphor. For Gd_2O_2S:Eu, MTF data were found comparable to those of Gd_2O_2S:Tb, while the MTF of Lu_2SiO_5:Ce was even higher resulting in better spatial resolution and image sharpness properties. On the other hand, Gd_2O_2S:Eu was found to exhibit higher output signal and zero-frequency detective quantum efficiency than Lu_2SiO_5:Ce.

Keywords: powder scintillators, x-ray mammography, radiation detectors, image quality

1. Introduction

Luminescent materials, either in the form of powder scintillators (phosphor screens) or crystals, are incorporated in many medical imaging radiation detectors. Powder scintillators are successfully employed in a large number of x-ray radiography devices (from conventional and digital x-ray radiography, mammography and x-ray computed tomography to positron tomography, digital dental radiography and portal imaging) (Arnold 1979, Yaffe and Rowlands 1997, Boone 2000, Van Eijk 2002, Nikl 2006). Among various materials, rare-earth-ion-doped oxyorthosilicates provide excellent scintillating properties and thus they have been extensively investigated for the development of new scintillators (Lee *et al* 2006). Physical characteristics of the Gd_2O_2S:Eu, Lu_2SiO_5:Ce, CsI:Tl and Gd_2O_2S:Tb scintillators are given in table 1.

Table 1. Physical characteristics of scintillators for medical imaging radiation detectors.

	Density (g cm^{-3})	$\rho Z_{\text{eff}}^4(10^6)$	Hygroscopicity	Light yield (photons/Mev)	Decay time (ns)	Emission maximum (nm)
Gd_2O_2S:Eu[a]	7.3	103	No	60 000	$\sim 1 \times 10^6$	623
Lu_2SiO_5:Ce[b]	7.4	143	No	26 000	40	420
CsI:Tl[b]	4.51	38	Slight	66 000	800–6000	550
Gd_2O_2S:Tb[b]	7.3	103	No	60 000	$\sim 1 \times 10^6$	545

[a]Data are from (Okumura *et al* 2002).
[b]Data are from (Van Eijk C W E 2002).

Terbium (Tb)-activated phosphors (i.e. Gd_2O_2S:Tb, La_2O_2S:Tb and Y_2O_2S:Tb) have been up to now accepted to be the most efficient x-ray-to-light converters (Arnold 1979, Gurwich 1995, Kandarakis *et al* 1996, Liaparinos *et al* 2007) employed in mammography and radiography. Currently the most widely used phosphors are Gd_2O_2S:Tb and CsI:Tl.

Gd_2O_2S:Tb has been proven very useful in conventional radiography screen-film systems, where precise matching of the spectral sensitivity of the x-ray film to the emission of the phosphor is of primary consideration in order to obtain the highest speed for the screen–film combination. However, in the past decade there has been an increasing tendency to introduce digital radiography and mammography systems (Rodnyi *et al* 2001, Van Den Bergh and Leblans 2005).

In some digital imaging systems, based on crystalline silicon (Si) optical detectors (CCDs, photodiodes), the green light emitted by terbium-activated phosphors is not very efficiently detected (Gurwich 1995). This is because a large number of Si-based devices, incorporated in x-ray imaging systems, are not adequately sensitive to these wavelengths (500–550 nm); only 45–55% of the light produced by Gd_2O_2S:Tb or Y_2O_2S:Tb is registered by the Si photodiode (Gurwich 1995).

Since most Si-based photodetectors are more sensitive to longer wavelengths, and particularly in the red wavelength range, it will be of interest to investigate the emission efficiency of red-emitting phosphors (Rodnyi *et al* 2001, Van Den Bergh and Leblans 2005).

For this purpose, europium (Eu)-activated phosphors, emitting at wavelengths toward the red region of the light spectrum, could be used instead of green-emitting Tb-activated phosphors (Gambaccini *et al* 1996). These red-emitting phosphors should also show adequate matching with some films exhibiting high sensitivity to red light, such as those used in laser imagers. Furthermore, the performance of many europium-doped scintillators, and particularly Gd_2O_2S:Eu, has been previously found comparable to terbium-activated phosphors (both showing 190% of the $CdWO_4$'s optical output). Gd_2O_2S:Eu has high light yield (60 000 photons/MeV) and luminescence efficiency, high density (7.3 g cm^{-3}), high radiation detection index ($\rho Z_{\text{eff}}^4 = 103 \times 10^6$) and finally decay time of the order of ms (slightly higher than Gd_2O_2S:Tb) which is acceptable for most x-ray radiography applications that do not involve high framing rates (Lempicki *et al* 2002, Okumura *et al* 2002, Nagarkar *et al* 2003, Michail *et al* 2008). These include stationary digital and conventional general radiography and mammography.

Lutetium oxyorthosilicate Lu_2SiO_5:Ce (LSO) is a scintillator with a number of advantages such as high light yield (26 000 photons/MeV) and luminescence efficiency, high density (7.4 g cm^{-3}), high radiation detection index ($\rho Z_{\text{eff}}^4 = 143 \times 10^6$), fast decay time (40 ns), high effective atomic number (66) and excellent chemical stability (Melcher and Schweitzer 1992a, 1992b, Blasse and Grabmaier 1994, Van Eijk 2002, Dorenbos *et al* 1995). Furthermore, Lu_2SiO_5:Ce emits light in the blue region which renders it compatible with a large number of optical sensors. In single crystal form, Lu_2SiO_5:Ce has already been used in several non-imaging applications such as gamma ray detection in nuclear physics, high energy physics and environmental monitoring (Melcher and Schweitzer 1992a, 1992b). Lu_2SiO_5:Ce has also replaced $Bi_4Ge_3O_{12}$ (BGO) scintillator in some positron emission tomography (PET) scanners. Lu_2SiO_5:Ce has lag problems leading to an increase in the fluorescence time. Lag is caused by the fact that the afterglow of this phosphor has two decay components, i.e. a fast component which is dominant in the first 40–50 ns and a slow component dominant beyond 100 ns. However, it may be used in digital x-ray breast tomosynthesis techniques (a technique for producing slice images using conventional x-ray systems) which use frame images with frame rates up to 2 images s^{-1}. Up to now, the CsI/a-Si flat-panel detector with $\sim$1000 ns primary decay has been used for breast tomosynthesis (Dobbins and Godfrey 2003). Gd_2O_2S:Eu probably cannot be used in such applications due to its long primary decay time.

In previous studies, Lu_2SiO_5:Ce was found to have better detection efficiency than Gd_2O_2S:Tb (David *et al* 2007, Liaparinos *et al* 2007) and comparable modulation transfer function (MTF) values (Liaparinos *et al* 2007, Michail *et al* 2007). However, Lu_2SiO_5:Ce in powder form (phosphor) has not yet been fully investigated.

The purpose of the present study was to compare an efficient blue-emitting powder phosphor (Lu_2SiO_5:Ce) with one of the most efficient red-emitting powder phosphors (Gd_2O_2S:Eu) in the mammographic energy range. For this purpose, we investigated spatial frequency dependent and single index image quality parameters such as the MTF, the zero-frequency detective quantum efficiency ($\eta_D(0)$), the noise equivalent passband (Ne) and the informational efficiency (η_I). In addition, the spectral compatibility of those materials with various detectors was estimated. Our results were also compared to published data concerning a well-known commercially employed Gd_2O_2S:Tb screen.

2. Materials and methods

2.1. Screen preparation

The phosphor materials, necessary for the experiments, were purchased in powder form (Phosphors Technology Ltd, England, codes: UKL63/N-R1 for Gd_2O_2S:Eu and ZBK58/N-S1 for Lu_2SiO_5:Ce, with a mean grain size of approximately 8 μm and a volume density of 7.3 and 7.4 g cm^{-3} respectively). The phosphors were used in the form of thin layers (test screens) to simulate the intensifying screens employed in x-ray mammography. For the purposes of the present study, a 25 mg cm^{-2} Lu_2SiO_5:Ce and a 33.1 mg cm^{-2} Gd_2O_2S:Eu thick scintillating screen were prepared by sedimentation of the powder phosphors on fused silica substrates (spectrosil B). Sodium orthosilicate (Na_2SiO_3) was used as a binding material between the powder grains. The sedimentation was achieved by using a mixture consisting of 1000 ml of de-ionized water, 20 ml of Na_2SiO_3 and the appropriate amount of phosphor powder in a glass tube of 110 cm height. The fused silica substrate was placed at the bottom of the tube (Giakoumakis *et al* 1990, Kandarakis *et al* 1997).

Experiments were performed on a General Electric Senographe DMR Plus x-ray mammographic unit with molybdenum anode target and molybdenum filter. Tube voltage was checked using an RMI model 240 multifunction meter. Incident exposure rate measurements were performed using a Radcal 2026C ionization chamber dosimeter (Radcal Co., USA).

2.2. Quantum detection efficiency (QDE)

The efficiency of a phosphor screen to detect x-ray photons is estimated by the quantum detection efficiency (QDE) (Boone 2000, Yaffe and Rowlands 1997). QDE is the fraction of incident photons interacting within the scintillator mass. For polyenergetic x-ray beams, QDE is averaged over the x-ray spectrum as follows:

$$\langle \eta_q \rangle_E = \frac{\int_0^{E_0} \Phi(E)(1 - e^{-(\mu_{\mathrm{tot},t}(E)/\rho)w_0})\,dE}{\int_0^{E_0} \Phi(E)\,dE}, \qquad (1)$$

where E denotes the x-ray photon energy, E_0 is the maximum energy of the x-ray spectrum, $\Phi(E)$ is the x-ray spectrum and $\mu_{\mathrm{tot},t}(E)/\rho$ is the x-ray total mass attenuation coefficient of the scintillator, computed using the corresponding values for Lu, Si, O, Gd and S as tabulated by Hubbell and Seltzer (1995). w_0 is the coating thickness of the phosphor screen (in units of mg cm^{-2}). The denominator in (1) expresses the total x-ray photon flux incident on the detector.

2.3. Output signal

The output signal was measured by performing x-ray exposure and emitted light energy flux measurements. Emitted light energy flux measurements were performed using an experimental setup comprising a light integration sphere (Oriel model 70451) coupled to a photomultiplier (EMI 9798B)

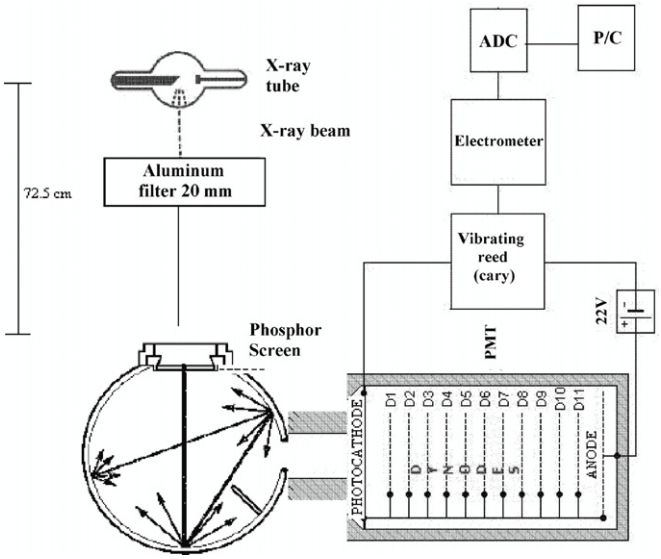

Figure 1. Experimental set-up for the measurement of the emitted light energy flux comprising the integrating sphere, the PMT and the vibrating reed electrometer.

connected to a Cary 401 vibrating reed electrometer (David *et al* 2007).

The photomultiplier was coupled to the output port of the integrating sphere, to reduce experimental errors due to illumination nonuniformities. The screen was positioned at the input port of the integrating sphere whereas the photomultiplier (PMT) was adapted at the output port (figure 1). The photocathode of the photomultiplier (extended S-20) was directly connected to a Cary 401 vibrating reed electrometer by bypassing all dynodes. In this manner, photocurrent instability and electronic noise amplification due to photomultiplier's dynode high voltage were avoided (Valais *et al* 2005).

The light flux of the screens was determined after corrections on the experimental data according to the following formula:

$$\dot{\Psi}_\Lambda = \frac{I_{\mathrm{elec}}}{\tau_0(s_{\mathrm{PC}}a_s)} \cdot \frac{1}{A_{\mathrm{sc}}}, \qquad (2)$$

where I_{elec} is the current at the output of the electrometer (in pA), s_{PC} is the peak photosensitivity of the photocathode (in pA W^{-1}), which was used as a factor converting the output photocathode current into light energy flux. a_s is the spectral matching factor of the screen's emission spectrum to the spectral sensitivity of the photocathode (extended S-20, see section 2.8). A_{sc} is the irradiated area of the screen. τ_0 denotes the throughput of the integration sphere, which is expressed by the ratio (Oriel 70451 Integrating sphere data sheet)

$$\tau_0 = \frac{\Psi_e}{\Psi_i} = \frac{\rho_o A_e/A_{\mathrm{sc}}}{1 - \rho_o(1 - A_p/A_{\mathrm{sc}})}, \qquad (3)$$

where Ψ_e is the total light flux at the exit (output) port of the integrating sphere, Ψ_i is the total flux at the input port, A_e is the area of the exit port, A_p is the sum of all port areas and ρ_o denotes the reflectance of the internal sphere wall. Using a series of prototype light-emitting diodes (LED, Kingbright Company) and by taking into account specific data (on A_e, A_{SC}, A_p, ρ_o) given by the manufacturer's datasheet, the throughput was calculated to be $\tau_0 = 15.6$.

2.4. Modulation transfer function (MTF)

The MTF was experimentally determined by the square wave response function (SWRF) method (Barnes 1979, Bunch *et al* 1987, ICRU 1986, Norman 2005). A Nuclear Associates resolution test pattern (typ-53, Nuclear Associates) containing Pb lines of various widths corresponding to various spatial frequencies (from 0.25 lp mm^{-1} to 10 lp mm^{-1}) was used to obtain pattern images. The screens were brought in close contact with radiographic films (Kodak T-Mat for Lu_2SiO_5:Ce and Agfa LT 2B for Gd_2O_2S:Eu) enclosed in a light tight cassette. The film–screen combinations were irradiated by x-rays at the mammographic unit. Reflection mode measurements were followed, i.e light emitted by the irradiated screen side was measured (the film was placed behind the test pattern and in front of the screen). Reflection mode represents the conventional mammography intensifying screens and the rear screens of an ordinary radiographic cassette.

After irradiation, films were developed in an Agfa Scopix LR 5200 film processor, operated at 36 °C and at 90 s processing time. Pattern images, obtained on the films, were digitized in an Agfa Duoscan scanner with scanning parameters 1000 dpi, 8 bit. Prior to digitization, it was verified that the film optical density values were within the linear part of the H&D characteristic curve. The MTF curves were finally determined from the digitized image optical density variations (digital CTF). The latter were obtained across directions vertical with respect to the test pattern lines, employing Coltman's formula, which gives the MTF as a function of CTF (Barnes 1979, ICRU 1986). CTF is given as (Efstathopoulos *et al* 2001)

$$\mathrm{CTF}(f) = \frac{I_{\max} - I_{\min}}{I_{\max} + I_{\min}}, \tag{4}$$

where $I_{\max}$ is the local maximum and $I_{\min}$ is the local contrast minimum for a given frequency. Given the CTF, the Coltman formula to determine the MTF is

$$\mathrm{MTF}(f) = \frac{\pi}{4}\left[C(f) + \frac{C(3f)}{3} - \frac{C(5f)}{5} + \frac{C(7f)}{7} + \cdots\right], \tag{5}$$

where $\mathrm{MTF}(f)$ is the sine wave MTF and $C(f)$ is the bar target CTF (Norman 2005, Williams *et al* 1999). The MTF data, obtained in this way, were corrected by dividing by the MTF of the scanner and the MTF of the films. The exposure conditions employed for the MTF measurements were 27 and 28 kVp for the Lu_2SiO_5:Ce and Gd_2O_2S:Eu screens respectively. These slightly different x-ray tube voltages correspond to the middle point of the linear part of the H&D curves.

2.5. Zero-frequency detective quantum efficiency (DQE(0))

Zero-frequency DQE expresses the signal-to-noise ratio $(\mathrm{SNR}_0/\mathrm{SNR}_I)^2$ squared. SNR_0 is the output signal-to-noise ratio, associated with the image produced by the detector, and SNR_I is the input signal-to-noise ratio, related to the incident x-ray beam (Dick and Motz 1981). DQE(0) was determined according to a method described in a previous study (Kandarakis *et al* 1998). Zero-frequency DQE was determined by employing a method based on luminescence and emission spectra measurements (Cavouras *et al* 2005, Kandarakis *et al* 1998). According to this method, DQE(0) has been expressed as follows:

$$\eta_D(0) = \frac{\eta_\psi[E/E_\lambda]}{(\eta_\psi[E/E_\lambda]/\eta_q) + 1}, \tag{6}$$

where η_ψ is the x-ray luminescence efficiency (XLE) ($\eta_\Psi = \Psi_\Lambda/\Psi_0$), which was determined after dividing the light energy flux, in (2), by the incident x-ray energy fluence (Ψ_0) (Cavouras *et al* 2005). The latter was found by converting x-ray exposure data to energy fluence (Boone 2000).

2.6. Noise equivalent passband (Ne)

Beyond the spatial frequency-dependent parameters, image quality can also be expressed by single indices. The following two parameters, called the noise equivalent passband (Ne) and the informational efficiency (η_I), provide such indices. Calculation of these parameters was based on the experimentally measured values of the MTF.

According to Wagner (1977), to compare systems with different MTFs and Nyquist frequencies, the approach of the noise equivalent passband should be adopted. The noise equivalent passband, expressing image sharpness by a single number, has been defined (Evans 1981) by

$$\mathrm{Ne} = \int_0^\infty \mathrm{MTF}^2(v)\,\mathrm{d}v. \tag{7}$$

Equation (7) describes Ne as a quantity proportional to the area under the curve of the MTF squared.

2.7. Informational efficiency (η_I)

Informational efficiency (η_I) compares the imaging performance of real imaging systems to the performance of perfect (ideal) systems (Dainty and Shaw 1974) by a single index. The informational efficiency has been defined (Dainty and Shaw 1974) as

$$\eta_I(E, w) = \frac{\eta_D(0)}{\eta_{D\,\mathrm{id}}(0)} \frac{\mathrm{Re}(E, w)}{\mathrm{Re}(E, w)_{\mathrm{id}}}, \tag{8}$$

where $\eta_D(0)$ is the zero-frequency detective quantum efficiency. The quantity Re has been defined (Dainty and Shaw 1974) as

$$\mathrm{Re}(E, w) = \int_0^\infty \mathrm{MTF}^2(v) v\,\mathrm{d}v, \tag{9}$$

where subscript 'id' denotes that $n_D(0)$ and Re correspond to an ideal imaging system. Since by definition $\eta_{D\mathrm{id}}(0) = 1$ and $\mathrm{MTF}(v)_{\mathrm{id}} = 1$, (8) is simplified to

$$\eta_I(E, w) = \eta_D(0)\mathrm{Re}(E, w) \Big/ \int_0^\infty v\,\mathrm{d}v. \tag{10}$$

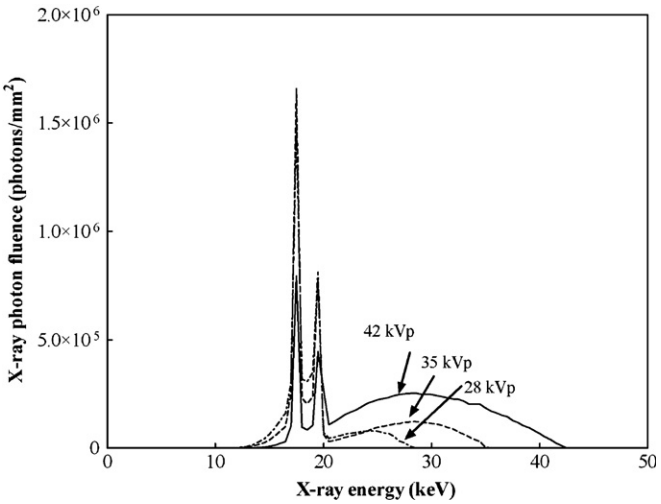

Figure 2. X-ray photon fluence spectra (photons mm^{-2}) filtered by a 30 mm additional Perspex block.

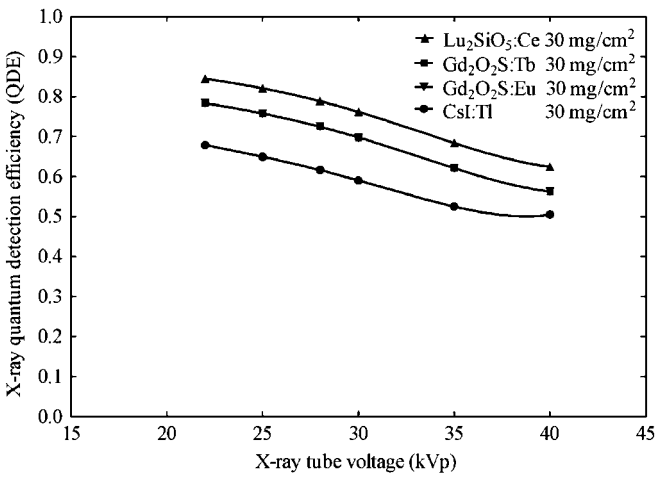

Figure 3. X-ray quantum detection efficiency (QDE) for the Lu_2SiO_5:Ce, Gd_2O_2S:Eu, CsI:Tl and Gd_2O_2S:Tb screens in the mammographic energy range.

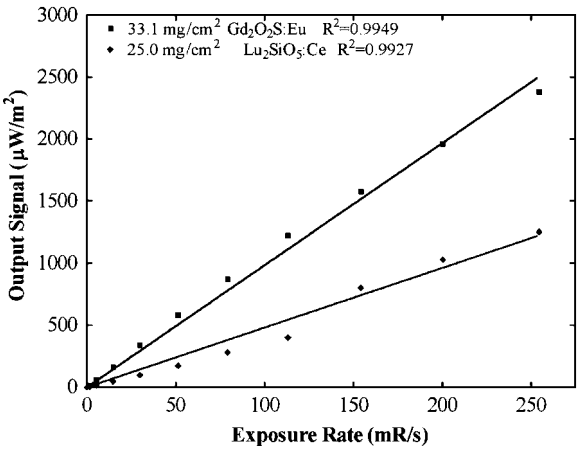

Figure 4. The characteristic curves of Lu_2SiO_5:Ce and Gd_2O_2S:Eu phosphors in the mammography range of exposures.

2.8. Spectral matching factor (a_s)

In medical imaging, where scintillating screens are used in combination with optical detectors (films, photocathodes, photodiodes), the spectral matching between the emitted phosphor light and the optical detector sensitivity must be taken into account. This is because the degree of spectral matching affects the amount of light utilized to form the final image. The spectral matching factor (a_s), which expresses the spectral compatibility to optical photon detectors, can be calculated by (11):

$$\alpha_S = \frac{\int \mathrm{Sp}(\lambda) S_D(\lambda)\,\mathrm{d}\lambda}{\int \mathrm{Sp}(\lambda)\,\mathrm{d}\lambda}, \qquad (11)$$

where $\mathrm{Sp}(\lambda)$ is the spectrum of the light emitted by the phosphor and $S_D(\lambda)$ is the spectral sensitivity of the optical detector coupled to the phosphor (Kandarakis *et al* 1997). To determine α_S, the emitted light spectra of the Gd_2O_2S:Eu and Lu_2SiO_5:Ce powder phosphors were measured using an Oriel grating optical spectrometer (Ocean Optics Inc., HR2000). The spectrum from a 5 mm thick CsI:Tl crystal scintillator (CRYOS Ltd, Ukraine) was also measured for comparison purposes. Spectrometer light measurements were performed under x-ray excitation.

3. Results and discussion

In figure 2, examples of x-ray spectra used in the calculations of QDE (equation (1)) are depicted. The vertical axis values correspond to incident x-ray photon fluence (Boone and Seibert 1997, Boone 2000).

The calculated results based on tabulated data for the x-ray quantum detection efficiency of Gd_2O_2S:Eu, Lu_2SiO_5:Ce, CsI:Tl and Gd_2O_2S:Tb are shown in figure 3. For comparison purposes, equal coating thickness (30 mg cm^{-2}) was assumed for all scintillators. As expected, the x-ray quantum detection efficiency decreases with increasing energy. For the same screen coating thickness, Lu_2SiO_5:Ce has higher quantum detection efficiency values than both Gd_2O_2S:Eu and Gd_2O_2S:Tb screens, as well as CsI:Tl, due to its higher total attenuation ($\mu_{\mathrm{tot},t}(E)/\rho$) coefficient ($cm^2\ g^{-1}$) values, calculated from tabulated data on attenuation coefficients of the chemical elements (Hubbell and Seltzer 1995). Gd_2O_2S:Tb and Gd_2O_2S:Eu have the same stopping power due to their equal attenuation coefficients (overlapping curves in figure 3). The different activators affect the emission spectra but, due to their low concentration, they do not affect the detection efficiency. However, for the coating thickness of the screens employed in the present study, where the Lu_2SiO_5:Ce screen is clearly thinner, QDE was found approximately equal for all screens.

The x-ray characteristic curves of Lu_2SiO_5:Ce and Gd_2O_2S:Eu (output signal versus incident exposure) are plotted in figure 4 and show a linear dependence between the output signal and the exposure rate in the 4.8–250 mR s^{-1} range. The linear no-threshold fit gave a reduced R^2 of 0.9927 for Lu_2SiO_5:Ce and 0.9949 for Gd_2O_2S:Eu, which are very close to the most likely reduced R^2 values and indicate that the screens have linear response in this energy range. Gd_2O_2S:Eu was found with clearly higher output signal values than those of Lu_2SiO_5:Ce. The ratio of the output signals

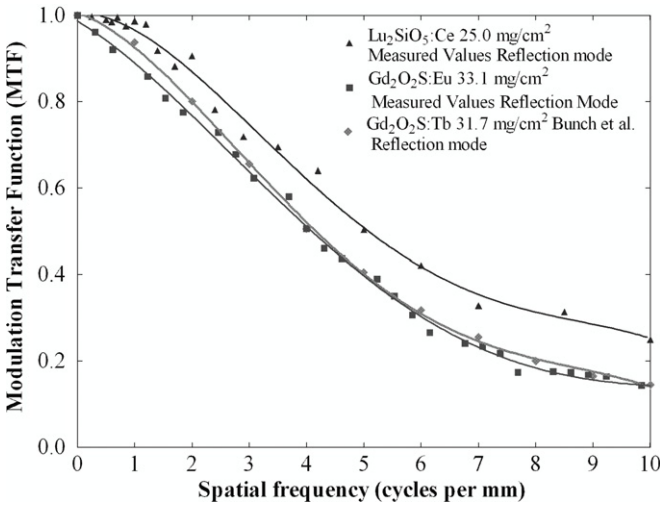

Figure 5. Comparison of the MTFs of Lu_2SiO_5:Ce, Gd_2O_2S:Eu and Gd_2O_2S:Tb employed in the Kodak Min-R screens as measured experimentally in reflection mode.

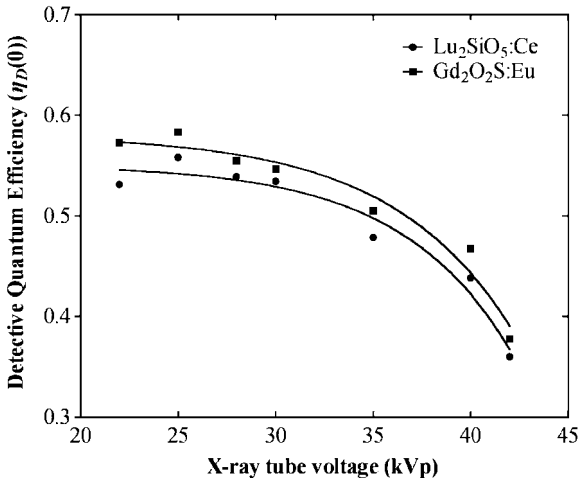

Figure 6. Variation of the zero-frequency detective quantum efficiency of the Lu_2SiO_5:Ce and Gd_2O_2S:Eu screens with x-ray tube voltage in the mammographic energy range.

(light yield per MeV), found in the present study for the two phosphors, is similar to previously published data, i.e. 26 000 photons/MeV for Lu_2SiO_5:Ce and 60 000 photons/MeV for Gd_2O_2S:Eu (Okumura *et al* 2002, Van Eijk 2002).

Figure 5 shows MTFs of the 25.0 mg cm^{-2} Lu_2SiO_5:Ce, the 33.1 mg cm^{-2} Gd_2O_2S:Eu and Gd_2O_2S:Tb employed in the 'Kodak Min-R film-screen system' (Bunch *et al* 1987). The Lu_2SiO_5:Ce screen was found to have higher MTF than the Gd_2O_2S:Eu and Gd_2O_2S:Tb screens, which however are thicker. This difference may be explained by (i) the lower thickness of the Lu_2SiO_5:Ce screen, since MTF decreases with increasing screen thickness due to the larger light spread into the phosphor mass, (ii) the lower light emission wavelength of Lu_2SiO_5:Ce, at 420 nm, i.e. the blue light emitted by the Lu_2SiO_5:Ce screen shows higher optical attenuation within the phosphor mass. Thus laterally directed photons (traveling longer distances to reach the screen surface) are strongly attenuated, resulting in reduced light spreading, sharper light output and improved spatial resolution.

The noise equivalent passband value for the Lu_2SiO_5:Ce screen was found to be 25.87. For Gd_2O_2S:Tb it was found to be 23.42 and for Gd_2O_2S:Eu 21.19. This difference may be explained by considering the lower values of the experimental MTFs corresponding to the Gd_2O_2S:Tb and Gd_2O_2S:Eu screens. The informational efficiency of Lu_2SiO_5:Ce was found to be 0.1843, which is clearly greater than that of Gd_2O_2S:Tb (0.1381) and Gd_2O_2S:Eu (0.1234). Likewise in noise equivalent passband, the superiority of Lu_2SiO_5:Ce is due to the higher MTF and DQE(0) values (see below). The corresponding values are listed in table 2.

Figure 6 shows the results for the variation of the zero-frequency detective quantum efficiency of the 25.0 mg cm^{-2} Lu_2SiO_5:Ce and the 33.1 mg cm^{-2} Gd_2O_2S:Eu screens with x-ray tube voltage in the mammographic energy range. DQE(0) was determined according to (6) via the measured E_λ, η_ψ and calculated η_q values. Gd_2O_2S:Eu showed higher DQE(0) than Lu_2SiO_5:Ce in the whole mammographic range due to its higher light flux and detection efficiency (for the 33.1 mg cm^{-2}) values and lower mean light photon energy (E_λ = 2.02 eV for Gd_2O_2S:Eu and 2.98 eV for Lu_2SiO_5:Ce). It should be noted that the theoretical maximum DQE at zero spatial frequency is limited by the x-ray quantum detection efficiency of the detector material (Dick and Motz 1981). In this sense, one could expect higher DQE(0) for Lu_2SiO_5:Ce. However, since Lu_2SiO_5:Ce emits lower light flux (output signal), its output signal-to-noise ratio and the corresponding DQE(0) are found reduced.

Table 2. Noise equivalent passband and informational efficiency.

	Noise equivalent passband	Informational efficiency
Lu_2SiO_5:Ce	25.87	0.1843
Gd_2O_2S:Eu	21.19	0.1234
Gd_2O_2S:Tb	23.42	0.1381

Figure 7 demonstrates optical spectra of four scintillators. Lu_2SiO_5:Ce emits in the blue region of the spectrum with a mean emission wavelength at 423 nm and can be combined with various films and some digital detectors (table 3). The Lu_2SiO_5:Ce spectrum is very similar to that measured by Lempicki and Globo (1998) for single crystal Lu_2SiO_5:Ce under different exposure conditions. Suzuki *et al* (1993) once proposed that the LSO lattice contains two sites for Lu ions with six and seven oxygen ligands and, correspondingly, two activator centers, $Ce^{3+}(1)$ and $Ce^{3+}(2)$. According to this model, the two emission peaks at 403 nm and 423 nm should belong to the $Ce^{3+}(1)$ emission from the excited 5d state to the ground state doublet $4f^1$ ($2F_{5/2}$ and $2F_{7/2}$) separated by about 2200 cm^{-1} (Rodriguez-Mendoza *et al* 2001). Furthermore, the broad wavelength band on the right-hand side of the spectrum might be due to partial contribution of $Ce^{3+}(2)$ center or due to inhomogeneous broadening of $Ce^{3+}(1)$ emission induced by inequivalent centers.

The Gd_2O_2S:Tb spectrum was obtained from previous reports (Kalivas *et al* 1999). Gd_2O_2S:Tb emits green light with a mean emission wavelength at 545 nm and has traditionally been used in conventional and digital x-ray imaging systems.

Table 3. The spectral matching factors of Lu_2SiO_5:Ce, Gd_2O_2S:Eu, CsI:Tl and Gd_2O_2S:Tb powder scintillators with some optical photon detectors currently used in conventional radiographic cassettes (screen films) and in digital detectors.

Optical detectors	Lu_2SiO_5:Ce	Optical detectors	Gd_2O_2S:Eu	Optical detectors	CsI:Tl[a]	Gd_2O_2S:Tb[a]
a-Si photodiode	0.62	a-Si photodiode	0.83	a-Si:H (104H)	0.77	0.91
CCD S100AB SITe®	0.87	CCD S100AB SITe®	0.97	CCD S100AB SITe®	0.93	0.92
AgfaGS	0.92	Agfa Scopix LT 2B	0.98	AGFA Ortho CP-G Plus	0.43	0.64
MAMORAY	0.87	APD Hamamatsu S5343 M = 50	1.00	c-Si (S1227-BR Hamamatsu)	0.81	0.79
KodakGR	0.96	Avalanche photodiode AD500-1.3G-TO5	0.95	c-Si (S1337-BR Hamamatsu)	0.56	0.55
FujiUM	0.90	Avalanche photodiode AD230-2.3G-TO5	0.94	GaAsP (Hamamatsu)	0.80	0.86
PSPMT Hamamatsu 8500	0.85	Wavelength selective photodiode WS-7 A1	0.93	CCD S100AF SITe®	0.69	0.67

[a] Data are from Kandarakis *et al* (2005).

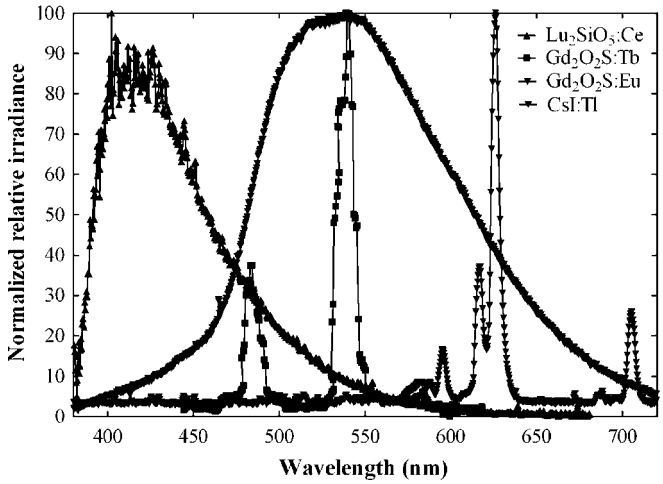

Figure 7. Emission spectra of Lu_2SiO_5:Ce, Gd_2O_2S:Eu, CsI:Tl and Gd_2O_2S:Tb phosphor screens.

Gd_2O_2S:Eu emits red light with a mean emission wavelength at 623 nm and can be combined mainly with electronic optical detectors such as CCDs, a-Si photodiodes and red sensitive films used in laser cameras (Rodnyi *et al* 2001, Van Den Bergh and Leblans 2005).

The emission spectrum peak of a CsI:Tl crystal was found at 545 nm. The CsI:Tl emission spectrum is well situated within the spectral sensitivities of optical detectors (photodiodes, photocathodes and charge coupled devices) frequently employed in radiation detectors (Nagarkar *et al* 2004).

4. Conclusions

In the present study, two powder scintillator screens, a 25.0 mg cm^{-2} Lu_2SiO_5:Ce and a 33.1 mg cm^{-2} Gd_2O_2S:Eu screen, were prepared and examined under x-ray mammography conditions. Screen performance was investigated through various parameters such as the output optical signal, the modulation transfer function as well as single index image quality parameters expressing image sharpness and the signal-to-noise ratio. Results were compared to similar data obtained for the commercially employed Gd_2O_2S:Tb phosphor. The Lu_2SiO_5:Ce screen was found with clearly higher MTF and image sharpness characteristics than both the Gd_2O_2S:Eu and the commercially used Kodak Min-R screen. However, Lu_2SiO_5:Ce is more expensive and has lower x-ray light flux and zero-frequency detective quantum efficiency than Gd_2O_2S:Eu. Gd_2O_2S:Eu has high light yield and can be used in digital detectors with spectral sensitivity in the red region of the spectrum and with red sensitive films currently employed in laser cameras instead of Gd_2O_2S:Tb and CsI:Tl, which were found with relatively lower spectral compatibility.

Note

Figures 4, 5 and 7 have been presented at the 2008 IEEE Workshop on Imaging Systems and Techniques and published in its proceedings.

Acknowledgment

The above work was funded by the Greek State Scholarships Foundation (I.K.Y.).

References

Arnold B A 1979 Physical characteristics of screen–film combinations *The Physics of Medical Imaging: Recording System, Measurements and Techniques* ed A G Haus (New York: American Association of Physicists in Medicine) p 30

Barnes G T 1979 *The Physics of Medical Imaging: Recording System, Measurements and Techniques* ed A G Haus (New York: American Association of Physicists in Medicine)

Blasse G and Grabmaier B C 1994 *Luminescent Materials* (Berlin: Springer)

Boone J M and Seibert J A 1997 An accurate method for computer-generating tungsten anode x-ray spectra from 30 to 140 kV *Med. Phys.* **24** 1661–70

Boone J M 2000 X-ray production, interaction, and detection in diagnostic imaging *Handbook of Medical Imaging* vol 1 ed J Beutel, H L Kundel and R L Van Metter (Bellingham: SPIE Press Physics and Psycophysics) p 40

Bunch P C, Huff K E and Van Meter R 1987 Analysis of the detective quantum efficiency of a radiographic screen–film combination *J. Opt. Soc. Am.* A **4** 902

Cavouras D *et al* 2005 Light emission efficiency and imaging performance of $Y_3Al_5O_{12}$: Ce (YAG: Ce) powder screens under diagnostic radiology conditions *Appl. Phys.* B **80** 923–33

Cunningham I A 2000 Applied linear systems theory *Handbook of Medical Imaging* vol 1 ed J Beutel, H L Kundel and R L Van Metter (Bellingham: SPIE Press Physics and Psycophysics) p 79

David S *et al* 2007 Efficiency of Lu_2SiO_5:Ce (LSO) powder phosphor as x-ray to light converter under mammographic imaging conditions *Nucl. Instrum. Methods Phys. Res.* A **571** 346–49

Dainty J C and Shaw R 1974 *Image Science* (New York: Academic) p 232

Dick E and Motz J W 1981 Image information transfer properties of x-ray fluorescent screens *Med. Phys.* **8** 337

Dobbins J T III and Godfrey D J 2003 Digital x-ray tomosynthesis: current state of the art and clinical potential *Phys. Med. Biol.* **48** R65–106

Dorenbos P, De Haas J T M and Van Eijk C W E 1995 Non-proportionality in the scintillation response and the energy resolution obtainable with scintillation crystals *IEEE Trans. Nucl. Sci* **42** 2190

Efstathopoulos E P, Costaridou L, Kocsis O and Panayiotakis G 2001 A protocol-based evaluation of medical image digitizers *Br. J. Radiol.* **74** 841

Evans A L 1981 *The Evaluation of Medical Images* (Bristol: Hilger)

Gambaccini M, Taibi A, Del Guerra A, Marziani M and Tuffanelli A 1996 MTF evaluation of a phosphor-coated CCD for x-ray imaging *Phys. Med. Biol.* **41** 2799

Giakoumakis G E, Nomicos C D, Yiakoumakis E N and Evangelou E K 1990 Absolute efficiency of rare earth oxysulfide screens in reflection mode observation *Phys. Med. Biol.* **35** 1017

Greening J R 1985 *Fundamentals of Radiation Dosimetry* (London: Institute of Physics)

Gurwich A M 1995 Luminescent screens for mammography *Radiat. Meas.* **24** 325

Hubbell J H and Seltzer S M 1995 Tables of x-ray mass attenuation coefficients and mass energy absorption coefficients 1 keV to 20 MeV for elements $Z = 1$ to 92 and 48 additional substances of dosimetric interest, US Department of commerce NISTIR 5632

ICRU (International Commission on Radiological Units) 1986 Modulation transfer functions of screen–film systems *ICRU Report No 41* (Bethesda, MD: ICRU)

Kalivas N, Costaridou L, Kandarakis I, Cavouras D, Nomicos C D and Panayiotakis G 1999 Effect of intrinsic-gain fluctuations on quantum noise of phosphor materials used in medical x-ray imaging *Appl. Phys.* A **69** 337

Kandarakis I, Cavouras D, Panayiotakis G S, Agelis T, Nomicos C D and Giakoumakis G S 1996 X-ray induced luminescence and spatial resolution of La_2O_2S:Tb phosphor screens *Phys. Med. Biol.* **41** 297–307

Kandarakis I, Cavouras D, Panayiotakis G S and Nomicos C D 1997 Evaluating x-ray detectors for radiographic applications: a comparison of ZnSCdS:Ag with Gd_2O_2S:Tb and Y_2O_2S:Tb screens *Phys. Med. Biol.* **42** 1351–73

Kandarakis I, Cavouras D, Kanellopoulos E, Nomicos C D and Panayiotakis G S 1998 Experimental determination of detector gain, zero frequency detective quantum efficiency, and spectral compatibility of phosphor screens: comparison of CsI:Na and Gd_2O_2S:Tb for medical imaging applications *Nucl. Instrum Methods Phys. Res.* A **417** 86

Kandarakis I *et al* 2005 Response of YAl_3O:Ce (YAG:Ce) powder scintillating screens to medical imaging x-rays *Nucl. Instrum Methods Phys. Res.* A **538** 615–30

Lee J K, Muenchausen R E, Lee J S, Jia Q X, Nastasi M, Valdez J A, Bennett B L and Cooke D W 2006 Structure and optical properties of Lu_2SiO_5:Ce phosphor thin films *Appl. Phys. Lett.* **89** 101905

Lempicki A and Globo J 1998 Ce-doped scintillators LSO and LuAP *Nucl. Instrum Methods Phys. Res.* A **414** 333–44

Lempicki A, Brecher C, Szupryczynski P, Lingertat H, Nagarkar V V, Tipnis S V and Miller S R 2002 A new lutetia-based ceramic scintillator for x-ray imaging *Nucl. Instrum Methods* A **488** 579–90

Liaparinos P, Kandarakis I, Cavouras D, Delis H and Panayiotakis G S 2007 Modeling granular phosphor screens by Monte Carlo methods *Med. Phys.* **33** 4502–14

Liaparinos P, Kandarakis I, Cavouras D, Delis H and Panayiotakis G S 2007 Monte Carlo study on the imaging performance of powder Lu_2SiO_5:Ce phosphor screens under x-ray excitation: comparison with Gd_2O_2S:Tb screens *Med. Phys.* **34** 1724–33

Melcher C L and Schweitzer J S 1992a A promising new scintillator: cerium doped lutetium oxyorthosilicate *Nucl. Instrum. Methods Phys. Res.* A **314** 212

Melcher C L and Schweitzer J S 1992b Cerium-doped lutetium oxyorthosilicate: a fast, efficient new scintillator *IEEE Trans. Nucl. Sci.* **39** 502

Michail C, David S, Liaparinos P, Valais I, Nikolopoulos D, Kalivas N, Toutountzis A, Cavouras D, Kandarakis I and Panayiotakis G S 2007 Evaluation of the imaging performance of LSO powder scintillator for use in x-ray mammography *Nucl. Instrum. Methods Phys. Res.* A **580** 558–61

Michail C, Valais I, Toutountzis A, Kalyvas N, Fountos G, David S, Kandarakis I and Panayiotakis G 2008 Light emission efficiency of (GOS:Eu) powder screens under x-ray mammography conditions *IEEE Trans. Nucl. Sci.* **55** 3703

Nagarkar V V, Tipnis S V, Miller S R, Lempicki A, Brecher C, Szupryczynski P and Lingertat H 2003 A new x-ray scintillator for digital radiography *IEEE Trans. Nucl. Sci.* **50** 297–300

Nagarkar V V, Tipnis S V, Gaysinskiy V, Miller S R and Shestakova I 2004 High speed digital radiography using structured CsI screens *Nucl. Instrum. Methods Phys. Res.* B **213** 476

Nikl M 2006 Scintillation detectors for x-rays *Meas. Sci. Technol.* **17** R37–54

Norman B N 2005 Test procedures for verifying IAFIS image quality requirements for fingerprint scanners and printers *MTR 05B0000016*

Okumura M, Tamatani M, Matsuda N, Takahara T and Fukuta Y 2002 Ceramic scintillator, method for producing same, and x-ray detector and x-ray CT imaging equipment using same *US Patent* No. 6,384,417

Oriel 70451 Integrating Sphere data sheet, Oriel Instruments, Internet site address http://www.spectraphysics.com/com/cda/products/all_products/0,1061,101188 00,00/

Rodnyi P A, Mikhrin S B, Mishin A N and Sidorenko A V 2001 Small-size pulsed x-ray source for measurements of scintillator decay time constants *IEEE Trans. Nucl. Sci.* **48** 2340

Rodriguez-Mendoza U R, Cunningham G B, Shen Y and Bray K L 2001 High-pressure luminescence studies in Ce^{3+}:Lu_2SiO_5 *Phys. Rev.* B **64** 195112

Suzuki H, Tombrello T A, Melcher C L and Schweitzer J S 1993 Light emission mechanism of $Lu_2(SiO_4)O$:Ce *IEEE Trans. Nucl. Sci.* **40** 380–3

Valais I, Kandarakis I, Nikolopoulos D, Sianoudis I, Dimitropoulos N, Cavouras D, Nomicos C and Panayiotakis G 2005 Luminescence efficiency of GdSiO:Ce scintillator under x-ray excitation *IEEE Trans. Nucl. Sci.* **52** 1830–35

Van Eijk C W E 2002 Inorganic scintillators in medical imaging *Phys. Med. Biol.* **47** R85–106

Van Den Bergh R and Leblans P 2005 Rare earth activated lutetium oxysulfide phosphor for direct x-ray detection *European Patent* No. EP1493798

Wagner R F 1977 Toward a unified view of radiological imaging systems: Part II. Noisy images *Med. Phys.* **4** 279–96

Williams M B, Simoni P U, Smilowitz L, Stanton M, Phillips W and Stewart A 1999 Analysis of the detective quantum efficiency of a developmental detector for digital mammography *Med. Phys.* **26** 2273

Yaffe M J and Rowlands J A 1997 X-ray detectors for digital radiography *Phys. Med. Biol.* **42** 1–39